Fate of charge order in overdoped La-based cuprates

Downloaded from: https://research.chalmers.se, 2026-09-16 19:09 UTC

Citation for the original published paper (version of record):
von Arx, K., Wang, Q., Mustafi, S. et al (2023). Fate of charge order in overdoped La-based cuprates. npj Quantum Materials, 8(1). http://dx.doi.org/10.1038/s41535-023-00539-w

N.B. When citing this work, cite the original published paper.

research.chalmers.se offers the possibility of retrieving research publications produced at Chalmers University of Technology. It covers all kind of research output: articles, dissertations, conference papers, reports etc. since 2004. research.chalmers.se is administrated and maintained by Chalmers Library

(article starts on next page)

ARTICLE OPEN

Check for updates

Fate of charge order in overdoped La-based cuprates

K. von Arx[1,2✉], Qisi Wang[1], S. Mustafi[1], D. G. Mazzone[3], M. Horio[4], D. John Mukkattukavil[5], E. Pomjakushina[6], S. Pyon[7], T. Takayama[8], H. Takagi[8,9], T. Kurosawa[10], N. Momono[10,11], M. Oda[10], N. B. Brookes[12], D. Betto[12], W. Zhang[13], T. C. Asmara[13], Y. Tseng[13], T. Schmitt[13], Y. Sassa[2] and J. Chang[1✉]

In high-temperature cuprate superconductors, stripe order refers broadly to a coupled spin and charge modulation with a commensuration of eight and four lattice units, respectively. How this stripe order evolves across optimal doping remains a controversial question. Here we present a systematic resonant inelastic x-ray scattering study of weak charge correlations in $La_{2-x}Sr_xCuO_4$ and $La_{1.8-x}Eu_{0.2}Sr_xCuO_4$. Ultra high energy resolution experiments demonstrate the importance of the separation of inelastic and elastic scattering processes. Long-range temperature-dependent stripe order is only found below optimal doping. At higher doping, short-range temperature-independent correlations are present up to the highest doping measured. This transformation is distinct from and preempts the pseudogap critical doping. We argue that the doping and temperature-independent short-range correlations originate from unresolved electron–phonon coupling that broadly peaks at the stripe ordering vector. In $La_{2-x}Sr_xCuO_4$, long-range static stripe order vanishes around optimal doping and we discuss both quantum critical and crossover scenarios.

npj Quantum Materials (2023)8:7 ; https://doi.org/10.1038/s41535-023-00539-w

INTRODUCTION

Charge order is now established in virtually all known hole underdoped cuprates[1–11], and hence is a universal property on equal footing with the pseudogap[12] and superconductivity. The evolution of charge order and the pseudogap beyond optimal doping has been challenging to establish. The pseudogap may emerge through a quantum critical transition[13–17], a cross-over phenomenon[18] or as a precursor to a symmetry breaking. It has also been difficult to establish a general trend as to how charge order evolves into the overdoped limit. In $(Bi,Pb)_{2.12}Sr_{1.88}CuO_{6+x}$ (Bi2201), a long-range charge ordering extending all the way to room temperature is reported in the overdoped regime beyond the doping extent of the pseudogap phase[19]. In the La-based cuprates, spin and charge stripe order around 1/8-doping are coupled[6,7,20–22]. Doping evolution of stripe order thus involves both spin and charge unless a doping-induced decoupling takes place. A recent study on $La_{1.6-x}Nd_{0.4}Sr_xCuO_4$ suggests that spin-stripe order persists across the entire superconducting dome[23] and long-range charge ordering outside the pseudogap phase has been reported in $La_{2-x}Sr_xCuO_4$ (LSCO)[24,25]. A resonant x-ray scattering study, by contrast, suggests that short-range charge correlations only exist inside the pseudogap phase[26]. Thus, contradicting observations on the charge order leave the questions of the coupling between spin and charge as well as a possible connection between charge order and the pseudogap unsolved.

Recently, Resonant Inelastic X-ray Scattering (RIXS) has been used to detect weak charge correlations by separating elastic from inelastic contributions[27]. In this fashion, charge correlations in $La_{1.8-x}Eu_{0.2}Sr_xCuO_4$ (LESCO) $x = 0.12$ were probed above the resonant elastic x-ray scattering onset temperature[11,28,29]. Here we use the RIXS sensitivity to trace charge correlations as a function of doping and temperature in LSCO and LESCO. Our main finding is the presence of long-range charge order for $x < 0.15$ and short-range correlations for $x > 0.15$. We show how the long-range charge order is strongly temperature and doping dependent while the short-range correlations are essentially doping and temperature independent. Our study provides a complete charge order phase diagram across optimal doping. Long-range charge correlation fades-out around optimal doping. Short-range charge correlations are found beyond optimal doping and seemingly beyond the pseudogap phase. We thus conclude that neither the long- nor short-range charge correlations correlate with the pseudogap phenomenon.

RESULTS

Charge order correlations

X-ray absorption spectra (XAS) across the copper *L*-edge for different doping concentrations *x* of LSCO are shown in the inset of Fig. 1a. Comparable data quality is obtained irrespective of doping and consistent with previous XAS studies of LSCO[30]. Example RIXS spectra on LSCO $x = 0.145$ and $x = 0.16$, recorded at the charge ordering wave vector for two different temperatures reveal scattering from elastic processes, phonon (70 meV), spin (~0.3 eV) and *dd* (1.8 eV) excitations (Fig. 1a, b). The phonon-, spin- and *dd*-contributions are consistent with previous RIXS studies[24,31]. A comparison of the two raw spectra shows that the elastic intensity is significantly enhanced at low temperature for $x = 0.145$ whereas elastic scattering appears temperature

[1]Physik-Institut, Universität Zürich, Winterthurerstrasse 190, CH-8057 Zürich, Switzerland. [2]Department of Physics, Chalmers University of Technology, SE-412 96 Göteborg, Sweden. [3]Laboratory for Neutron Scattering and Imaging, Paul Scherrer Institut, CH-5232 Villigen, PSI, Switzerland. [4]Institute for Solid State Physics, The University of Tokyo, Kashiwa, Chiba 277-8581, Japan. [5]Department of Physics and Astronomy, Uppsala University, Box 516, 751 20 Uppsala, Sweden. [6]Paul Scherrer Institut, CH-5232 Villigen, PSI, Switzerland. [7]Department of Applied Physics, The University of Tokyo, Tokyo 113-8646, Japan. [8]Max Planck Institute for Solid State Research, 70569 Stuttgart, Germany. [9]Department of Physics, The University of Tokyo, Tokyo 113-0033, Japan. [10]Department of Physics, Hokkaido University, Sapporo 060-0810, Japan. [11]Department of Applied Sciences, Muroran Institute of Technology, Muroran 050-8585, Japan. [12]European Synchrotron Radiation Facility, B.P. 220, 38043 Grenoble, France. [13]Swiss Light Source, Photon Science Division, Paul Scherrer Institut, CH-5232 Villigen, PSI, Switzerland. ✉email: karin.vonarx@uzh.ch; johan.chang@physik.uzh.ch

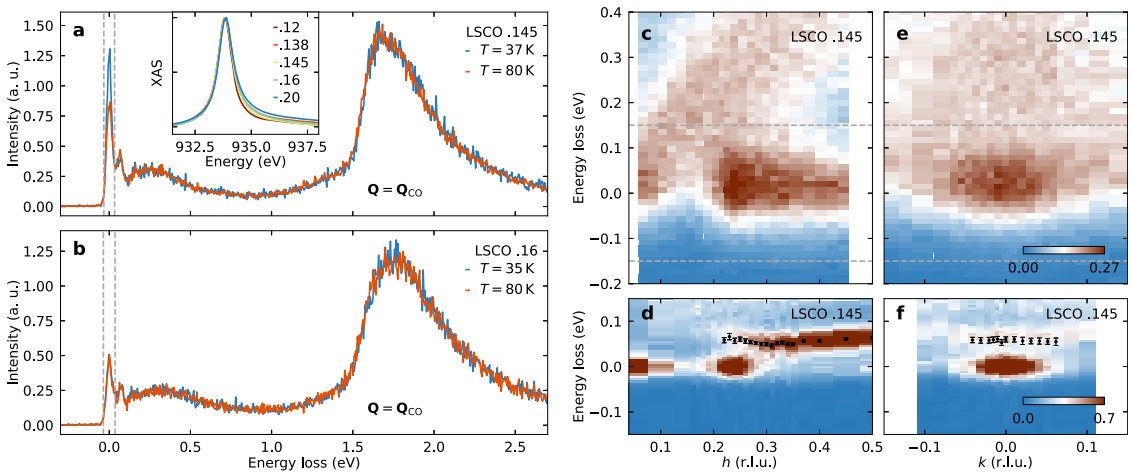

Fig. 1 X-ray absorption and resonant inelastic x-ray scattering spectra recorded on $La_{2-x}Sr_xCuO_4$ as a function of energy loss and momentum. a, b High-resolution RIXS spectra recorded on LSCO $x = 0.145$ and 0.16 at the charge ordering vector for different temperatures as indicated. Vertical dashed lines indicate the energy resolution and with that the integration window of elastic scattering. The intensity is given in arbitrary units (a. u.). The inset shows XAS spectra featuring the copper *L*-edge for LSCO with doping concentrations as indicated. **c–f** RIXS spectra probed in longitudinal (*h*) and transverse (*k*) directions on LSCO $x = 0.145$. Data in **c**, **e** are recorded with an energy resolution of 129 meV, whereas **d**, **f** show spectra recorded at a high-resolution beamline with a total resolution of 33 meV. Horizontal dashed lines in **c**, **e** illustrate the energy range in **d**, **f**. The improved resolution allows for resolving the phonon branch. The black circles mark the phonon dispersion determined from fitting the spectra. Error bars are set by standard deviation from fitting. High-resolution data were taken at 37 K, all other data at base temperature, see the "Methods" section.

independent for $x = 0.16$. The momentum dependence of elastic and inelastic scattering recorded on LSCO $x = 0.145$ is shown in Fig. 1c–f for longitudinal (*h*) and projected transverse (*k*) directions. In Fig. 1c, e data are recorded with an overall energy resolution of 129 meV (FWHM), whereas in d, f the resolution is 33 meV. The direct comparison illustrates how the quasielastic scattering in c and e includes both elastic and phonon responses. Since the intensity from the charge order peak and the phonon branch are comparable, differentiation can only be reached by applying sufficiently high energy resolution. Lack of sufficient energy resolution implies a convolution of charge order and phonon scattering intensities. The optical phonon branch, extracted from the high-resolution data of LSCO $x = 0.145$ in Fig. 1d and of LSCO $x = 0.16$ in supplementary Fig. 3 shows a dispersion behavior consistent with previous studies[24,31].

In what follows, quasielastic intensity is defined by integrating the RIXS intensity in a window set by the respective energy resolution around zero energy loss—see Fig. 1a. In this fashion, longitudinal and transverse elastic scans through the charge order vector were carried out for LSCO ($x = 0.12$, 0.138, 0.145, 0.16, and 0.2) and LESCO ($x = 0.125$, and 0.21) crystals. A linear background was subtracted. As shown in Fig. 2a, stripe order in LESCO $x = 0.125$ manifests by a reflection at $Q = (\delta, 0)$ with $\delta = 0.23$, as previously reported[27]. At optimal doping ($x \sim 0.16$ shown in Fig. 2d, g) and in the overdoped limit, represented by LSCO $x = 0.20$ (Fig. 3d, e) and LESCO $x = 0.21$ (Supplementary Fig. 2), much less elastic scattering is found.

For longitudinal (*h*) scans recorded with medium resolution, the convolution of charge order and phonon scattering leads to a double peak structure (Fig. 2b, c). The peak at $(h, 0) \approx (1/3, 0)$ stems from the optical phonon mode, likely in combination with absorption effects for large values of *h*. In transverse (rocking) scans, illustrated in the inset of Fig. 2e, the charge order peak appears with an additional broadening (Fig. 2f, g). Once sufficient energy resolution to filter out the optical phonon contribution is applied, the double peak structure disappears in the longitudinal scans and sharper peaks are found in the transverse scans. The medium resolution data on its own would therefore lead to a misinterpretation of charge order parameters like incommensurability and correlation length. This comparison shows the importance of high-resolution inelastic experiments as a probe of weak charge order away from 1/8 doping.

From long-range order to short-range correlations

In between 1/8 and optimal doping, our longitudinal scans show a decreasing elastic scattering intensity as doping is gradually increased. The evolution in doping shows a distinct transition in the nature of the charge correlation when the temperature dependence is taken into account. In Fig. 3a–e, we display the temperature dependence for the LSCO $x = 0.138$, 0.145, 0.16, and 0.20 compounds. For $x > 0.15$, essentially no temperature dependence is observed up to 150 K. We note that these two compounds have been recorded with different energy resolution. Supplementary Fig. 5 therefore compares the two compounds directly for medium- and high-resolution measurements. Together with the data for LSCO 0.145 in Figs. 1c–f and 2g it is revealed that the phonon contribution in the medium resolution *k* scans is only leading to a broadening of the peak while leaving the amplitude the same. Since the RIXS phonon intensity shows essentially no doping dependence for LSCO $x = 0.12 - 0.21$[24], the almost identical medium-resolution scans for $x = 0.16$ and 0.20 lead to the conclusion that the elastic scattering must behave similarly. It can therefore be inferred from the absent temperature dependence in high-resolution LSCO $x = 0.16$ scans, that there is indeed no temperature dependence for $x = 0.20$ as well. By contrast, for LSCO $x = 0.138$ and 0.145 a pronounced temperature dependence is found. The charge order intensity is suppressed with increasing temperature for $T > T_c$. The long-range charge order is also partially suppressed for $T < T_c$ in LSCO $x = 0.145$ due to phase competition with superconductivity[21,26]. By contrast, the short-range charge correlations appear insensitive to phase competition with superconductivity (Fig. 3c–e). This imposes a picture of two types of charge order: one long-range order that decays with temperature and short-range temperature-independent correlations. Our study provides a very narrow doping sector for the transition from temperature-dependent long-range order to temperature-independent short-range correlations between 0.145 and 0.16 doping. In fact, the transition may happen through a quantum critical point at $x \approx 0.15$. In Fig. 4a–c, we show how the incommensurability δ, correlation length ξ and integrated

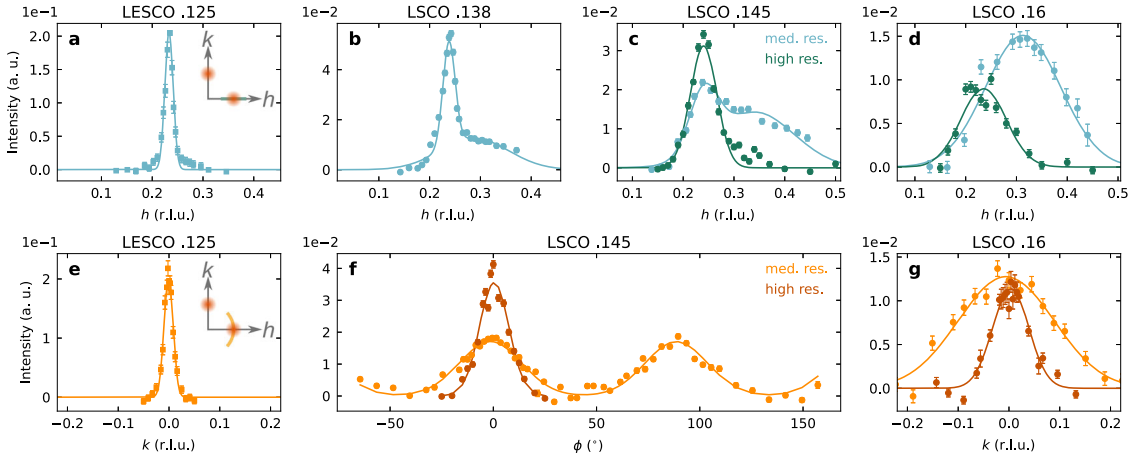

Fig. 2 Doping evolution of the charge order in LSCO and LESCO at base temperature. a–d Longitudinal scans along $(h, 0)$ for the compounds and compositions as indicated. **e, g** Transverse scans through the longitudinal peak position (δ, k) for doping concentrations as indicated. **f** Circular arc scan through two charge order reflections, with $\phi = 0$ at $(h, 0)$. Panels for LSCO $x = 0.145$ and 0.16 compare high- and medium- resolution data. Solid lines are Gaussian fits. Error bars are set by counting statistics. See text for further explanations. Insets display sketches of the charge order reflections in reciprocal space and the scan trajectories. Data in **a**, **e** are adapted from ref. [27].

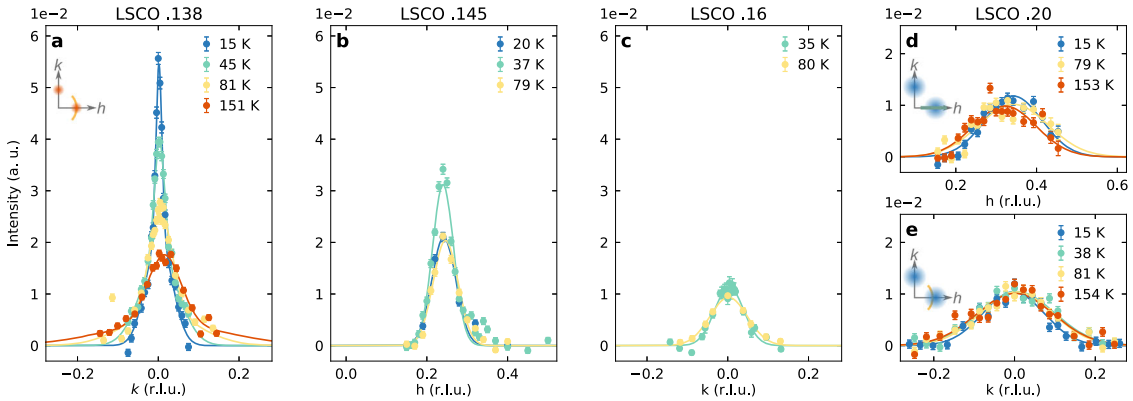

Fig. 3 Charge order temperature and doping dependence. a–e Transverse and longitudinal scans through the charge ordering vector $(\delta, 0)$ recorded as a function of temperature, as indicated, on LSCO $x = 0.138$, 0.145, 0.16, and 0.20. Data in **b**, **c** were recorded with high energy resolution, whereas in **a**, **d**, **e** medium resolution was applied, see text for further information. Solid lines are fits using a Gaussian lineshape. All intensities have been normalized to the integrated *dd*-excitation intensity. Error bars are set by counting statistics. Insets in **a**, **d**, **e** display the longitudinal and transverse scan direction.

intensity I/ξ^2 evolve from 1/8 to the overdoped regime. While the integrated intensity I/ξ^2 is roughly independent of doping, the correlation length declines as $x \to 0.15$. At the same time, we observe that $\delta \to 1/4$ for $x \to 0.15$. Beyond $x = 0.15$, the temperature-independent charge correlations hold similar integrated weight and incommensurability. Their correlation length of 10 Å corresponds to about three in-plane lattice parameters.

DISCUSSION

Several contradicting studies of stripe order in overdoped La-based cuprates have been published recently[23–26,32,33]. At 1/8 doping, charge order in LESCO could be detected above the onset temperature of the low-temperature tetragonal (LTT) phase[34] and above the transport onset of the pseudogap[35]. As a function of doping, long-range charge order has been reported even outside the pseudogap phase of LSCO[24,25]. Another study reported short-range charge correlations to exist within the pseudogap phase only and long-range charge order only around 1/8-doping[26]. Our comprehensive inelastic study suggests short-range correlations at low temperatures for $x > 0.15$ that persist across the pseudogap critical doping. The long-range stripe order by contrast decays fast as $x \to 0.15$. Our study therefore also contrasts the recent study reporting long-range charge order in LSCO, up to $x = 0.21$[24], despite using the same measurement technique. Neither of the short or long-range charge correlations reported here seem to connect with the psesudogap phase. A recent magneto-transport experiment across the low-temperature pseudogap "critical" point[36] suggests a symmetry breaking Fermi surface transformation. This is not easily reconciled with charge order correlations[37]. In the first place, it is difficult to envision how short-range charge correlations can impact the electronic structure and produce a Fermi surface transformation[38].

The here reported high-resolution RIXS data on LSCO provide a different picture than the existing literature that is mutually inconsistent. Our results resemble what has been reported in $YBa_2Cu_3O_{7-x}$ (YBCO). High-resolution RIXS measurements on YBCO and $Nd_{1+x}Ba_{2-x}Cu_3O_{7-\delta}$ reveal that the short-range correlations stem from quasi-elastic scattering processes[39–42]. Also in LSCO, it is not inconceivable that the short-range correlations result from dynamic charge fluctuations, for example, due to electron–phonon coupling of a low-energy phonon branch. In fact, recent high-resolution O *K*-edge RIXS experiments on optimally doped LSCO indicate strong electron–phonon coupling

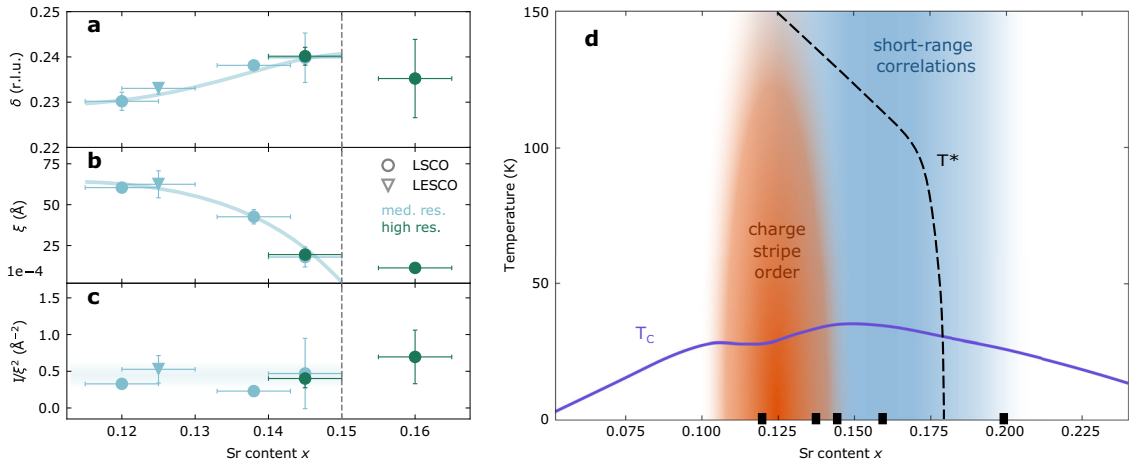

Fig. 4 Charge order parameters and phase diagram. a–c Charge order incommensurability δ, correlation length ξ (defined as the inverse half-width-half-maximum) and integrated diffracted intensity (amplitude I divided by ξ^2) versus hole doping for LSCO (circles) and LESCO (squares) at base temperature. The parameters were extracted from fits to elastic scans, see Supplementary Fig. 4. Error bars reflect the standard deviation obtained from the fits. Data for LSCO $x = 0.12$ are from ref. [53] and for LESCO $x = 0.125$ from ref. [27]. All colored lines are guides to the eye. Vertical dashed line in **a**–**c** marks the critical doping separating long- from short-range correlations. **d** Schematic charge order phase diagram: temperature versus hole doping/Sr content x. Superconducting dome and pseudogap onset of LSCO are illustrated by respectively solid violet and dashed black line[21,26,35]. Red and blue phases indicate respectively long-range and short-range charge correlations. Solid squares indicate the doping compositions studied in this work.

at a low-energy phonon branch around $(h, 0) = (1/4, 0)$[43]. Just as in LSCO, the short and long-range charge correlations in YBCO and $Nd_{1+x}Ba_{2-x}Cu_3O_{7-\delta}$ occur with a very similar scattering vector. As long demonstrated, charge order in LSCO and YBCO differ by their respective ordering vectors $Q_{CO} \approx (1/4, 0)$[6] and $\approx (1/3, 0)$[44]. The fact that the short-range correlations are so aligned with the long-range ordering strongly suggests a direct link. If the short-range charge correlations should be understood from electron–phonon coupling, this could also be the case for long-range ordering.

Now that similar short- and long-range charge correlations have been observed in both LSCO and YBCO, we discuss possible interpretations. The most prevailing view is that the long-range correlations manifest static charge order. The outstanding question is whether the short-range correlations are also static or in fact dynamic of nature. A transition from static long- to short-range correlations implies a crossover phenomenon. Should the short-range correlation however be dynamic in nature, then the long-range static order would occur through a quantum phase transition. Recent high-resolution O K-edge RIXS experiments hint to a dynamic nature of the short-range correlations and thus favors the quantum critical scenario[43]. Yet, future experiments with even better energy resolution are needed to clarify the issue. Another experimental route to confirm quantum criticality is to induce long-range order using an external tuning parameters such as hydrostatic pressure or magnetic field.

Another important question is why the La-214 and Y/Nd-1237 systems display different long-range incommensurabilities[45]. A possibility is that the detailed crystal structure generates different electron–phonon couplings[46]. Recently, it was shown how electron–phonon coupling is enhanced inside the low-temperature tetragonal (LTT) crystal structure of LESCO[31]—suggesting that electron–phonon coupling assists in the formation of long-range stripe order.

We conclude by commenting on the fact that the charge order incommensurabilities in LSCO and YBCO have opposite doping dependencies. If electron–phonon coupling is solely responsible for charge ordering, a more universal picture would be expected. It is therefore conceivable that electron–electron coupling also plays an important role. In the La-based cuprates, many experimental results point to a strong coupling picture which would support the electron–electron interaction hypothesis. Irrespective of the responsible interactions, our observation of a charge order vanishing around optimally doped LSCO provides new perspectives. It opens for a unified picture of charge order as similar results are found in YBCO. Critical fluctuations around the optimal doping may also have bearing in superconductivity and strange metal properties.

METHODS

Samples

High quality single crystals of LESCO and LSCO were grown using a floating zone method. These crystals have been used in previous studies[1,3,27,32,47,48]. All crystals were prealigned ex situ using x-ray LAUE backscattering and cleaved in situ by a standard top-post technique.

Resonant inelastic x-ray scattering

RIXS experiments were carried out at the ADvanced RESonant Spectroscopies (ADRESS)[49,50] beamline of the Swiss Light Source (SLS) at the Paul Scherrer Institut and the ID32 RIXS beamline at the European Synchrotron Radiation Facility (ESRF)[51]. Fixed angles of 130° and 149.5° between incident and scattered light was used for measurements at ADRESS and ID32, respectively. To determine zero energy loss, the low-energy part of each RIXS spectrum is analyzed as shown in Supplementary Fig. 1: Elastic scattering and a phonon excitation are fitted using Gaussian profiles where the width is set by the instrumental energy resolution. A damped harmonic oscillator response function is adopted to model the magnetic excitations and a quadratic function is added to mimic the background (BG). The intensity of each spectrum is normalized to the integrated intensity of the dd excitations. Given the quasi-two-dimensional character of this system, we consider only the in-plane momentum transfer which can be controlled by varying the incident angle θ and sample azimuthal angle ϕ. Wave vector **Q** at (q_x, q_y, q_z) is defined as $(h, k, l) = (q_x a/2\pi, q_y b/2\pi, q_z c/2\pi)$ reciprocal lattice units (r.l.u.) using pseudo-tetragonal notation, with $a \approx b \approx$ 3.79 Å and $c \approx 13.1$ Å. Energy resolution, expressed in full-width-at-half-maximum (FWHM) ranges from ≈122 to 129 meV for ADRESS data and ≈33 meV for the ID32 data. Momentum resolution was ≈0.006 r.l.u. for ADRESS data and ≈0.01 r.l.u. for the ID32 data, which is in both cases much smaller than the width

of the charge order peak. Across all experiments, base temperature was in the range of ~15–25 K.

DATA AVAILABILITY

All data supporting the findings in this study are present in the figures and/or the Supplementary Information. Additional raw experiment data is available in ref. [52].

Received: 23 May 2022; Accepted: 9 January 2023;
Published online: 19 January 2023

REFERENCES

1. Laliberté, F. et al. Fermi-surface reconstruction by stripe order in cuprate superconductors. *Nat. Commun.* **2**, 432 (2011).
2. Wu, T. et al. Magnetic-field-induced charge-stripe order in the high-temperature superconductor $YBa_2Cu_3O_y$. *Nature* **477**, 191–194 (2011).
3. Chang, J. et al. Direct observation of competition between superconductivity and charge density wave order in $YBa_2Cu_3O_{6.67}$. *Nat. Phys.* **8**, 871–876 (2012).
4. Ghiringhelli, G. et al. Long-range incommensurate charge fluctuations in (Y,Nd) $Ba_2Cu_3O_{6+x}$. *Science* **337**, 821–825 (2012).
5. Tabis, W. et al. Charge order and its connection with Fermi-liquid charge transport in a pristine high-T_c cuprate. *Nat. Commun.* **5**, 5875 (2014).
6. Tranquada, J. M., Sternlieb, B. J., Axe, J. D., Nakamura, Y. & Uchida, S. Evidence for stripe correlations of spins and holes in copper oxide superconductors. *Nature* **375**, 561–563 (1995).
7. Hücker, M. et al. Stripe order in superconducting $La_{2-x}Ba_xCuO_4$ ($0.095 \leqslant x \leqslant 0.155$). *Phys. Rev. B* **83**, 104506 (2011).
8. Achkar, A. J. et al. Distinct charge orders in the planes and chains of ortho-III-ordered $YBa_2Cu_3O_{6+\delta}$ superconductors identified by resonant elastic x-ray scattering. *Phys. Rev. Lett.* **109**, 167001 (2012).
9. Thampy, V. et al. Rotated stripe order and its competition with superconductivity in $La_{1.88}Sr_{0.12}CuO_4$. *Phys. Rev. B* **90**, 100510(R) (2014).
10. Comin, R. et al. Charge order driven by Fermi-arc instability in $Bi_2Sr_{2-x}La_xCuO_{6+\delta}$. *Science* **343**, 390–392 (2014).
11. Achkar, A. J. et al. Nematicity in stripe-ordered cuprates probed via resonant x-ray scattering. *Science* **351**, 576–578 (2016).
12. Norman, M. R., Pines, D. & Kallin, C. The pseudogap: friend or foe of high T_c? *Adv. Phys.* **54**, 715–733 (2005).
13. Daou, R. et al. Broken rotational symmetry in the pseudogap phase of a high-T_c superconductor. *Nature* **463**, 519–522 (2010).
14. Hashimoto, M. et al. Direct spectroscopic evidence for phase competition between the pseudogap and superconductivity in $Bi_2Sr_2CaCu_2O_{8+\delta}$. *Nat. Mater.* **14**, 37–42 (2015).
15. Horio, M. et al. Three-dimensional Fermi surface of overdoped La-based cuprates. *Phys. Rev. Lett.* **121**, 077004 (2018).
16. Michon, B. et al. Thermodynamic signatures of quantum criticality in cuprate superconductors. *Nature* **567**, 218–222 (2019).
17. Gupta, N. K. et al. Vanishing nematic order beyond the pseudogap phase in overdoped cuprate superconductors. *Proc. Natl Acad. Sci. USA* **118**, e2106881118 (2021).
18. Tallon, J. L., Storey, J. G., Cooper, J. R. & Loram, J. W. Locating the pseudogap closing point in cuprate superconductors: Absence of entrant or reentrant behavior. *Phys. Rev. B* **101**, 174512 (2020).
19. Peng, Y. Y. et al. Re-entrant charge order in overdoped $(Bi,Pb)_{2.12}Sr_{1.88}CuO_{6+\delta}$ outside the pseudogap regime. *Nat. Mater.* **17**, 697–702 (2018).
20. Tranquada, J. M. et al. Neutron-scattering study of stripe-phase order of holes and spins in $La_{1.48}Nd_{0.4}Sr_{0.12}CuO_4$. *Phys. Rev. B* **54**, 7489–7499 (1996).
21. Chang, J. et al. Tuning competing orders in $La_{2-x}Sr_xCuO_4$ cuprate superconductors by the application of an external magnetic field. *Phys. Rev. B* **78**, 104525 (2008).
22. Lake, B. et al. Antiferromagnetic order induced by an applied magnetic field in a high-temperature superconductor. *Nature* **415**, 299–302 (2002).
23. Ma, Q. et al. Parallel spin stripes and their coexistence with superconducting ground states at optimal and high doping in $La_{1.6-x}Nd_{0.4}Sr_xCuO_4$. *Phys. Rev. Res.* **3**, 023151 (2021).
24. Lin, J. Q. et al. Strongly correlated charge density wave in $La_{2-x}Sr_xCuO_4$ evidenced by doping-dependent phonon anomaly. *Phys. Rev. Lett.* **124**, 207005 (2020).
25. Miao, H. et al. Charge density waves in cuprate superconductors beyond the critical doping. *npj Quantum Mater.* **6**, 31 (2021).
26. Wen, J. J. et al. Observation of two types of charge-density-wave orders in superconducting $La_{2-x}Sr_xCuO_4$. *Nat. Commun.* **10**, 3269 (2019).
27. Wang, Q. et al. High-temperature charge-stripe correlations in $La_{1.675}Eu_{0.2}Sr_{0.125}CuO_4$. *Phys. Rev. Lett.* **124**, 187002 (2020).
28. Fink, J. et al. Charge ordering in $La_{1.8-x}Eu_{0.2}Sr_xCuO_4$ studied by resonant soft x-ray diffraction. *Phys. Rev. B* **79**, 100502(R) (2009).
29. Fink, J. et al. Phase diagram of charge order in $La_{1.8-x}Eu_{0.2}Sr_xCuO_4$ from resonant soft x-ray diffraction. *Phys. Rev. B* **83**, 092503 (2011).
30. Brookes, N. B. et al. Stability of the zhang-rice singlet with doping in lanthanum strontium copper oxide across the superconducting dome and above. *Phys. Rev. Lett.* **115**, 027002 (2015).
31. Wang, Q. et al. Charge order lock-in by electron-phonon coupling in $La_{1.675}Eu_{0.2}Sr_{0.125}CuO_4$. *Sci. Adv.* **7**, eabg7394 (2021).
32. Frachet, M. et al. Hidden magnetism at the pseudogap critical point of a cuprate superconductor. *Nat. Phys.* **16**, 1064–1068 (2020).
33. Lee, S. et al. Generic character of charge and spin density waves in superconducting cuprates. *Proc. Natl Acad Sci USA* **119**, e2119429119 (2022).
34. Klauss, H.-H. et al. From antiferromagnetic order to static magnetic stripes: the phase diagram of $(La, Eu)_{2-x}Sr_xCuO_4$. *Phys. Rev. Lett.* **85**, 4590–4593 (2000).
35. Cyr-Choinière, O. et al. Pseudogap temperature T^* of cuprate superconductors from the nernst effect. *Phys. Rev. B* **97**, 064502 (2018).
36. Fang, Y. et al. Fermi surface transformation at the pseudogap critical point of a cuprate superconductor. *Nat. Phys.* **18**, 558–564 (2022).
37. Collignon, C. et al. Thermopower across the phase diagram of the cuprate $La_{1.6-x}Nd_{0.4}Sr_xCuO_4$: signatures of the pseudogap and charge density wave phases. *Phys. Rev. B* **103**, 155102 (2021).
38. Millis, A. J. & Norman, M. R. Antiphase stripe order as the origin of electron pockets observed in 1/8-hole-doped cuprates. *Phys. Rev. B* **76**, 220503 (2007).
39. Arpaia, R. et al. Dynamical charge density fluctuations pervading the phase diagram of a Cu-based high-T_c superconductor. *Science* **365**, 906–910 (2019).
40. Wahlberg, E. et al. Restored strange metal phase through suppression of charge density waves in underdoped $YBa_2Cu_3O_{7-\delta}$. *Science* **373**, 1506–1510 (2021).
41. Yu, B. et al. Unusual dynamic charge correlations in simple-tetragonal $HgBa_2CuO_{4+\delta}$. *Phys. Rev. X* **10**, 021059 (2020).
42. Arpaia, R. & Ghiringhelli, G. Charge order at high temperature in cuprate superconductors. *JPSJ* **90**, 111005 (2021).
43. Huang, H. Y. et al. Quantum fluctuations of charge order induce phonon softening in a superconducting cuprate. *Phys. Rev. X* **11**, 041038 (2021).
44. Vinograd, I. et al. Locally commensurate charge-density wave with three-unit-cell periodicity in $YBa_2Cu_3O_y$. *Nat. Commun.* **12**, 3274 (2021).
45. Blackburn, E. et al. X-ray diffraction observations of a charge-density-wave order in superconducting ortho-II $YBa_2Cu_3O_{6.54}$ single crystals in zero magnetic field. *Phys. Rev. Lett.* **110**, 137004 (2013).
46. Banerjee, S., Atkinson, W. A. & Kampf, A. P. Emergent charge order from correlated electron-phonon physics in cuprates. *Commun. Phys.* **3**, 161 (2020).
47. Choi, J. et al. Unveiling unequivocal charge stripe order in a prototypical cuprate superconductor. *Phys. Rev. Lett.* **128**, 207002 (2022).
48. Ivashko, O. et al. Damped spin excitations in a doped cuprate superconductor with orbital hybridization. *Phys. Rev. B* **95**, 214508 (2017).
49. Ghiringhelli, G. et al. SAXES, a high resolution spectrometer for resonant x-ray emission in the 400-1600eV energy range. *Rev. Sci. Instrum.* **77**, 113108 (2006).
50. Strocov, V. N. et al. High-resolution soft X-ray beamline ADRESS at the Swiss Light Source for resonant inelastic X-ray scattering and angle-resolved photoelectron spectroscopies. *J. Synchrotron Radiat.* **17**, 631–643 (2010).
51. Brookes, N. et al. The beamline ID32 at the ESRF for soft x-ray high energy resolution resonant inelastic x-ray scattering and polarisation dependent x-ray absorption spectroscopy. *Nucl. Instrum. Methods Phys. Res.* **903**, 175–192 (2018).
52. von Arx, K. et al. Dataset for publication "The fate of charge order in overdoped La-based cuprates". Zenodo https://doi.org/10.5281/zenodo.7501723 (2023).
53. Wang, Q. et al. Uniaxial pressure induced stripe order rotation in $La_{1.88}Sr_{0.12}CuO_4$. *Nat. Commun.* **13**, 1795 (2022).

ACKNOWLEDGEMENTS

We thank D. LeBeouf and M.-H. Julien for discussions and comments to the manuscript. Part of the experiments have been performed at the ADRESS beamline of the Swiss Light Source at the Paul Scherrer Institut (PSI). We acknowledge Eugenio Paris for support at the beamline. K.v.A., Q.W., M.H., T.S., Y.T., and J.C. acknowledge support by the Swiss National Science Foundation through Grant Numbers BSSGI0-155873, 200021-188564, CRSII2_160765/1 and 200021-178867. K.v.A. is grateful for the support from the FAN Research Talent Development Fund - UZH Alumni. K.v.A. and Q.W. thank the Forschungskredit of the University of Zurich, grant no. [FK-21-105] and [FK-20-128]. Y.S. thanks the Chalmers Area of Advances-Materials Science and the Swedish Research Council (VR) with a starting Grant (Dnr. 2017-05078) for funding. T.C.A. acknowledges funding from the European Union's Horizon 2020 research and innovation programme under the Marie Skłodowska-Curie grant agreement No. 701647 (PSI-FELLOW-II-3i program). The synchrotron experiments

were performed at the Paul Scherrer Institut under proposal no. 20191754/20201779 and the ESRF under proposal no. HC-4422.

AUTHOR CONTRIBUTIONS

T.K., N.M., M.O., and E.P. grew the LSCO single crystals, whereas S.P., T.T., and H.T. synthesized LESCO single crystals. Q.W., K.v.A., S.M., M.H., D.M., N.B.B., D.B., W.Z., T.C.A., Y.T., Y.S., D.G.M., T.S., and J.C. carried out the RIXS experiments. K.v.A. analyzed the data with support from Q.W. and J.C. K.v.A. and J.C. wrote the manuscript with input from all authors.

COMPETING INTERESTS

The authors declare no competing interests.

ADDITIONAL INFORMATION

Supplementary information The online version contains supplementary material available at https://doi.org/10.1038/s41535-023-00539-w.

Correspondence and requests for materials should be addressed to K. von Arx or J. Chang.

Reprints and permission information is available at http://www.nature.com/reprints

Publisher's note Springer Nature remains neutral with regard to jurisdictional claims in published maps and institutional affiliations.

Open Access This article is licensed under a Creative Commons Attribution 4.0 International License, which permits use, sharing, adaptation, distribution and reproduction in any medium or format, as long as you give appropriate credit to the original author(s) and the source, provide a link to the Creative Commons license, and indicate if changes were made. The images or other third party material in this article are included in the article's Creative Commons license, unless indicated otherwise in a credit line to the material. If material is not included in the article's Creative Commons license and your intended use is not permitted by statutory regulation or exceeds the permitted use, you will need to obtain permission directly from the copyright holder. To view a copy of this license, visit http://creativecommons.org/licenses/by/4.0/.

© The Author(s) 2023